Rietveld Analysis of Nano-crystalline $MnFe_2O_4$ with Electron Powder Diffraction

Jin-Gyu Kim, Jung-wook Seo,* Jinwoo Cheon,‡ and Youn-Joong Kim*

Division of Electron Microscopic Research, Korea Basic Science Institute, Daejeon 305-333, Korea
**E-mail: y-jkim@kbsi.re.kr*
**Plating Technology Group, Samsung Electromechanics, Suwon 443-743, Korea*
‡Department of Chemistry, Yonsei University, Seoul 120-749, Korea
Received August 27, 2008, Accepted November 25, 2008

The structure of nano-crystalline $MnFe_2O_4$ was determined and refined with electron powder diffraction data employing the Rietveld refinement technique. A nano-crystalline sample (with average crystal size of about 10.9 nm) was characterized by selected area electron diffraction in an energy-filtering transmission electron microscope operated at 120 kV. All reflection intensities were extracted from a digitized image plate using the program ELD and then used in the course of structure refinements employing the program FULLPROF for the Rietveld analysis. The final structure was refined in space group $Fd\text{-}3m$ (# 227) with lattice parameters a=8.3413(7) Å. The reliability factors of the refinement are R_P=7.98% and R_B=3.55%. Comparison of crystallographic data between electron powder diffraction data and reference data resulted in better agreement with ICSD-56121 rather than with ICSD-28517 which assumes an initial structure model.

Key Words: Nano-crystalline $MnFe_2O_4$, Rietveld analysis, Electron powder diffraction, Energy filtering, Image plate

Introduction

The structure of nano-crystalline materials has been extensively studied during the last decades. The synthesis of nano-structured magnetic materials has become a particularly important area of research and is attracting growing interest because of the potential applications to ferrofluids, advanced magnetic materials, catalysts, colored pigments, high-density magnetic recording media, and medical diagnostics.[1-3] The substance $MnFe_2O_4$, one of the most important magnetic materials, has been widely used in electronic applications, information storage, magnetic resonance imaging (MRI) technology, and drug-delivery technology.[4-11] However, in order to develop synthetic methods for novel nano-crystals and to study their chemical and physical processes that occur on the nano-scale, it is required to apply appropriate analytical methods for determining the chemical composition and atomic structure of nano-sized materials.

X-ray powder diffraction is the most useful analysis method for determining the structure of bulk samples. However, the standard X-ray powder diffraction of nano-crystalline materials does not provide the sufficient intensity data necessary to determine the crystallographic information and perform structure refinement. Hence, additional methods are required to achieve the structure analysis of nano-crystalline materials.

Recently, Weirich *et al.*[12,13] have successfully determined and refined the nano-crystalline anatase (TiO_2) from electron powder diffraction data using the Rietveld technique. In the case of electron diffraction, the scattering power for electrons is about 10^6 times stronger than that for X-rays. Electron diffraction is, therefore, more suitable than X-ray diffraction for the structure determination of nano-crystalline materials.

In this study, we report the structure determination of nano-crystalline $MnFe_2O_4$ with energy-filtered electron powder diffraction using the Rietveld refinement technique.

Experimental Section

Synthesis of nano-crystalline $MnFe_2O_4$. We synthesized $MnFe_2O_4$ nano-particles using previously reported procedures.[14] Iron tris-2,4-pentadionate (Aldrich) and manganese chloride (Aldrich) precursors were mixed in an equivalence ratio of 2:1, and reacted in 20 ml of an octyl ether solvent containing oleic acid and oleyl amine at 290°C for 1 hour. The $MnFe_2O_4$ nano-particles (~10 mg) with desired sizes of 10 nm were dissolved in 1 ml of toluene and 2,3-dimercaptosuccinic acid (DMSA, ~10 mg) molecules were dissolved in 1 ml of methanol. We mixed these two solutions and allowed them to react at ~25°C overnight. After isolation of black powders through centrifugation, we added 1 ml of water and then adjusted the pH of the solution ~7.

TEM measurements. The as-prepared powder was intimately dispersed in ethanol and then was loaded as a droplet of the prepared suspension on an ultra thin carbon-supported Cu grid and air-dried. Energy-filtered electron powder dif-

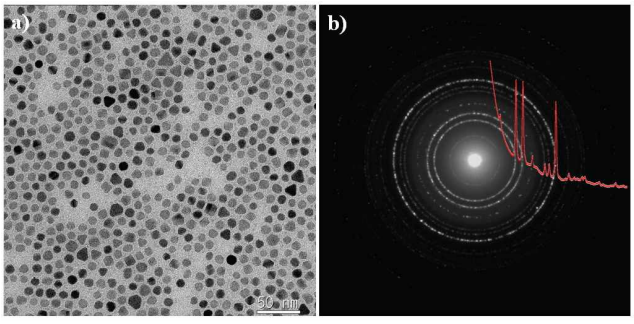

Figure 1. Bright-field image of $MnFe_2O_4$ nano-crystalline and the corresponding selected area electron powder diffraction. The overlay on the electron diffraction shows the average intensity profile that was used to determine the structure.

fraction was recorded on DITABIS imaging plates using the Carl Zeiss EM912 Ω transmission electron microscope. The microscope was operated at 120 kV with a zero-loss window of 15 eV. The digitized images (Figure 1) were calibrated for the camera constant and astigmatism with a diffraction pattern of a nano-crystalline gold standard sample and quantified by the program ELD (Calidris, Sollentuna, Sweden). High resolution transmission electron microscopy (HRTEM) images were obtained using the KBSI-HVEM (JEM-ARM 1300S, 1250 kV, 1.2 Å).

Results

For the structure determination with electron powder diffraction data, it is essential to carry out several steps of analysis procedures as follows: (i) extraction of the intensity profile and data processing, (ii) peak search and determination of the initial structure, (iii) extracting structure-factor amplitudes from the intensity profile, and (iv) structure refinement.

Extraction of intensity profile and data processing. In order to find peak positions, average radial intensity curves from the electron powder diffraction were obtained using the program ELD. The d-space of intensity curves were converted to two-theta (2θ) diffraction angles for each image pixel according to a simple formula

$$\theta = \arcsin(\lambda/2d),\ Rd = \lambda L,$$

where λ is the electron wavelength, R is the pixel number of a data point from the center of the diffraction pattern, and L is the corrected camera length in the digitized image.

Peak search and determination of initial structure. Analysis of the average intensity profile (Figure 2) using the peak-search tool in the program WinPLOTR[15] yielded 13 peaks between 0.3° and 2.4° in 2θ range. These peak positions were used as input for the program CRYSFIRE,[16] which is an automatic program for finding the unit cell and linked to several indexing programs, such as TREOR, DICVOL, and ITO12. As a result, its basic structure is a cubic system with lattice parameters a = 8.4764 Å. Determination of the most likely space groups was achieved by the program CHECKCELL.[17] For better screening of the space groups, additional 6 peaks were added to the initial 13 peaks (Figure 2). The best solutions resulted in three space groups: *Fd*-3*m* (#227), *F*-43*c* (#219), and *Fm*-3*c* (#226). In the case of two space groups *F*-43*c* and *Fm*-3*c*, their first peaks appeared at much lower angles compared to the experimental data. The initial structure of $MnFe_2O_4$ nano-crystalline, therefore, was determined to be space group *Fd*-3*m*, with lattice parameters a = 8.4764 Å. It was accorded to ICSD-28517 (a = 8.511(5) Å, *Fd*-3*m*).[18]

Extracting structure-factor amplitudes and Rietveld refinement. The Rietveld refinement of the average intensity profile of nano-crystalline $MnFe_2O_4$ was carried out using the program FULLPROF.[19] The inherent parameters determined by the standard Au data and other experimental parameters were used as input data in the program FULLPROF. The atomic scattering factors for X-ray were modified for electrons.[20] Usually, the atomic scattering factor for electrons is defined in the Mott-Bethe formula

$$f^e(s) = \frac{|e|}{16\pi^2\varepsilon_0|s|^2}\left[Z - f^X(s)\right],$$

where $f^e(s)$ is the atomic scattering factors for electrons, e is elementary charge, ε_0 is permittivity of vacuum, s is the scattering vectors, Z is the atomic number, and $f^X(s)$ is the atomic scattering factors for X-ray. The best source of electron scattering factors is that due to the Doyle-Turner parameterization

$$f^e(s) = 0.04787801\sum_{j=1}^{4} a_j e^{-b_j s^2}.$$

Thus, the Rietveld refinement should be performed correctly by applying the accurate values for two coefficients a_j and b_j for all atoms of Mn, Fe, and O in the program.

The first refinement cycles were used to adjust the back-

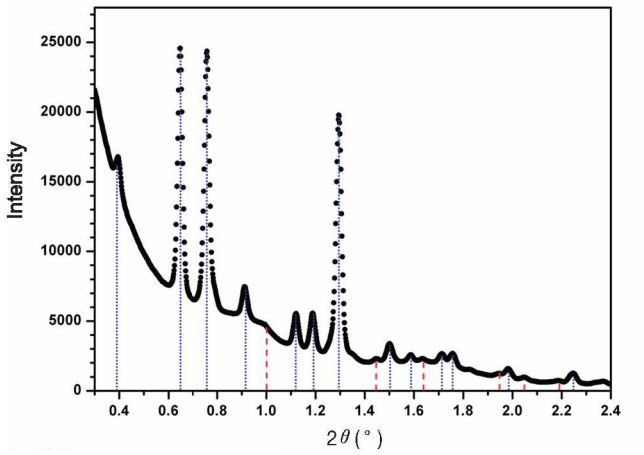

Figure 2. Average intensity profile to determine the unit cell and solve the initial structure. Peak positions indicated by thin blue dots (13 reflections) and additional thick red dashes (6 reflections) are used for determination of the unit cell and space group.

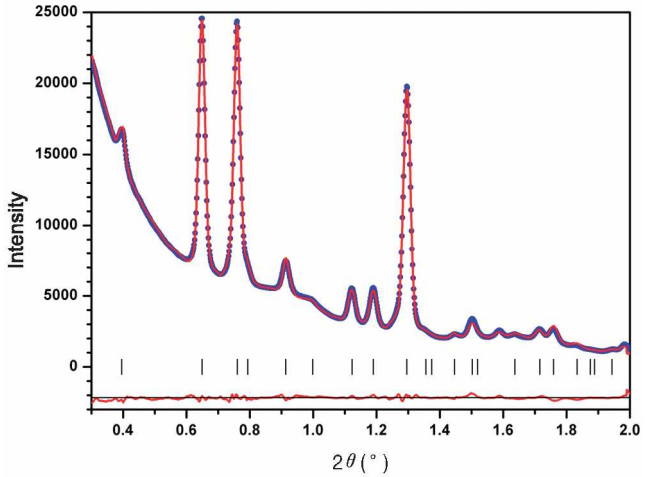

Figure 3. Rietveld analysis of the electron powder diffraction from $MnFe_2O_4$ nano-crystalline. The positions of the Bragg reflections are indicated by vertical bars (|). The difference between the experimental (dots) and the calculated (solid line) intensities from the refined model is shown by the plot in the lower part of the diagram.

Table 1. Crystallographic data and refinement results of $MnFe_2O_4$ nano-crystalline by the Rietveld analysis.

Formula, Z	$MnFe_2O_4$, 8
Space group	*Fd*-3*m* (#227)
Lattice parameters (Å)	a = 8.3413(7)
Cell volume (Å^3)	580.36(8)
D_{cal} (g cm^{-3})	5.274
Atomic sites	
Mn site	16*d*
Position (x, y, z)	0.625, 0.625, 0.625
SOF, B (Å^2)	0.46, 1.346(75)
Fe1 site	16*d*
Position (x, y, z)	0.625, 0.625, 0.625
SOF, B (Å^2)	0.54, 1.346(75)
Fe2 site	8*a*
Position (x, y, z)	0.0, 0.0, 0.0
SOF, B (Å^2)	1.0, 1.204(55)
O site	32*e*
Position (x, y, z)	0.3704(4), 0.3704(4), 0.3704(4)
SOF, B (Å^2)	1.0, 5.453(392)
Wavelength (Å)	0.03334
2θ scan range (°)	0.3 – 2.0
2θ scan step (°)	0.00168
No. of reflections	28
No. of parameters refined	14
R_p (%)	7.18
R_{wp} (%)	5.83
R_{exp} (%)	4.113
R_B (%)	3.55
R_F (%)	7.98
GOF-index	1.4

Table 2. Crystallographic data of $MnFe_2O_4$ crystal from the Inorganic Crystal Structure Database (ICSD).

Crystal system	Cubic (fcc)	
Lattice parameters	a = 8.402 Å	
Space group	*Fd* -3 *m*	
Atomic coordinates & SOF	Mn	0.625, 0.625, 0.625, 0.5
	Fe1	0.625, 0.625, 0.625, 0.5
	Fe2	0.000, 0.000, 0.000, 1.0
	O	0.380, 0.380, 0.380, 1.0

ground by a polynomial function of sixth order and for refining lattice parameters, the overall scale factor (level of intensity profiles), and zero shift. A Pearson-VII profile function[21] was employed to model the peak shape of the Bragg reflections. In the final step, atomic coordinates and isotropic displacement parameters B could be improved. The structure refinement was stable at all stages and converged rapidly to the results summarized in Table 1. The calculated and experimental diffraction profiles are shown in Figure 3 together with the difference curve obtained after the final refinement.

The final refinement of the electron diffraction data results in the lattice parameters a = 8.3413(7) Å. This value is somewhat different from the data in the initial structure, but agrees more closely with ICSD data of No.56121[22] (Table 2). This difference is affected by occupancy variation of Fe and Mn atoms, which occurred by substitution of Fe^{2-} and Mn^{2+} in the Fe_3O_4 structure. In order to refine the occupancy of the Fe and Mn atoms, refinement of the O atoms was first performed.

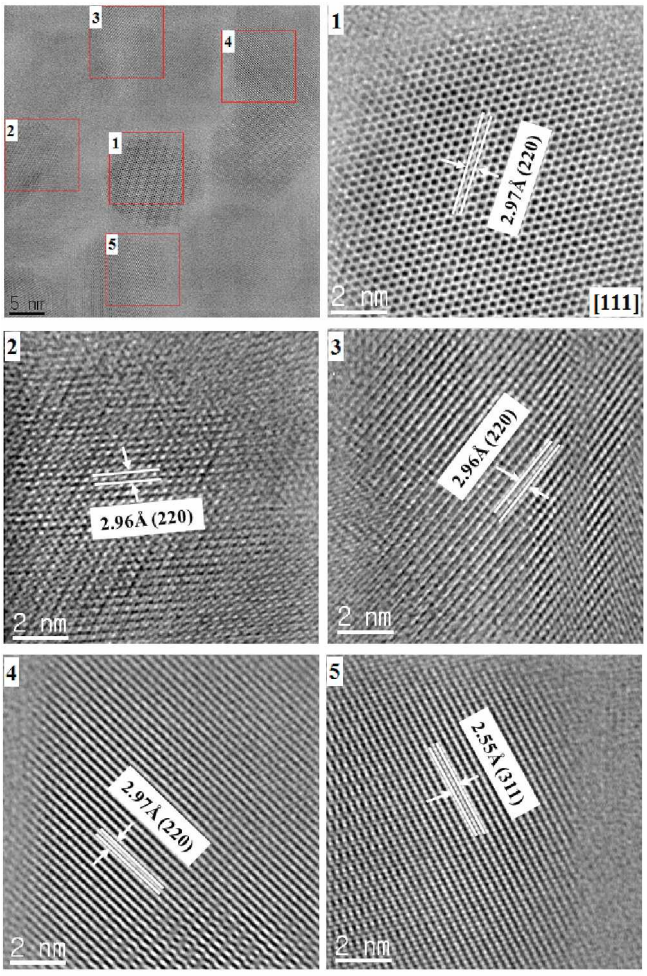

Figure 4. HRTEM images of $MnFe_2O_4$ nano-particles shown in Figure 1. Most lattice planes correspond to the (220) plane of $MnFe_2O_4$ nano-crystals.

Refinement of the Mn atoms was followed using the way which replaces the site of the Mn atoms with the Wyckoff site of the Fe atoms, 8*a*, 16*d*, in the Fe_3O_4 structure. As shown in Table 1, the Mn atoms were replaced with the Wyckoff site of the Fe atoms 16*d* from final refinement results. The occupancy ratio of Mn to Fe atoms at the Wyckoff site 16*d* is about 0.46:0.54. The chemical content ratio of Mn to Fe atoms in the unit cell is approximately 1:2.23, which agrees well with the result of the energy dispersive spectrometer (EDS) analysis (1:2.42). All these refinement results for the atomic coordinates and occupancy agree better with ICSD data of No. 56121 than with ICSD data of No. 28517.

Discussion

Effects of preferred orientation of nano-crystalline. In comparison with previous reports using the X-ray diffraction for the nano-rods and single particles of $MnFe_2O_4$,[23,24] the (220) and (440) reflections in our electron diffraction data presented relatively stronger intensities compared to other reflections. It was expected that those anomalous intensities originated from preferred orientation of $MnFe_2O_4$ nano-crystalline monodispersed on the TEM grids, since electron diffraction patterns

were formed by interaction between the specimen and the incident electron beam nearly parallel to the specimen. To evaluate the effects of the preferred orientation, the Rietveld refinement was carried out together with preferred orientation correction for the <110> direction. As a result, agreement of the experimental intensity profile with the calculated intensity profile was improved. To confirm the crystal structure and the preferred orientation, HRTEM images of $MnFe_2O_4$ were obtained. Figure 4 displays HRTEM images of $MnFe_2O_4$ nano-particles, indicating that most nano-crystallites include the (220) plane in common. Considering the interaction between incident beam and specimen, the Bragg angles are usually no more than 1° in forming HRTEM images. Therefore, it was expected that $MnFe_2O_4$ nano-crystals took a preferred orientation having (220) plane parallel to the incident beam, which resulted in enhancement of the (220) and (440) intensities.

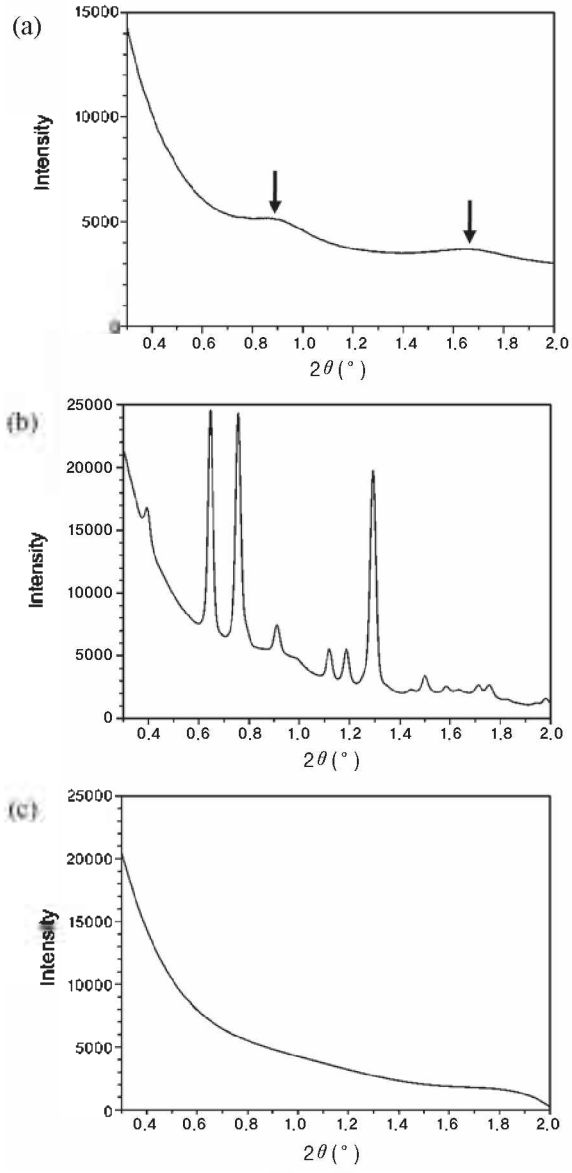

Figure 5. (a) Intensity profile from the C-supporting film excluding $MnFe_2O_4$ nano-crystalline. (b) Experimental intensity profile from $MnFe_2O_4$ nano-crystalline laid on the C-supporting film. (c) Polynomial function used in background subtraction.

Consideration of background intensity from C-supporting film. The polynomial function used to subtract the background intensity in the Rietveld analysis is

$$y_{bi} = \sum_{m=0}^{5} B_m \left(\frac{2\theta}{BKPOS} - 1 \right)^m$$

where y_{bi} is the back ground intensity, B_m is the background coefficient, and $BKPOS$ is the origin of the background position.

In fact, the electron powder diffraction from $MnFe_2O_4$ includes the diffuse scattering intensity from the C-supporting film. The intensity profile of amorphous diffraction from the C-supporting film is shown in Figure 5a. It has two shoulder peaks at 0.88° and 1.66° in the 2θ range. Figure 5b shows the observed intensity profile used for the final refinement and Figure 5c displays the polynomial function employed to subtract the background intensity from Figure 5b in the final refinement process. As shown in Figure 5c, intensities of two peaks from the C-supporting film could not be subtracted completely by the polynomial function. The intensities of these peaks, therefore, affect directly the profile matching between the observed and calculated intensity profiles in the course of structure factor quantification of the $MnFe_2O_4$ structure. To avoid these effects, it is necessary to remove manually the diffuse scattering intensity from the observed intensity profile before background subtraction using the polynomial function. Eventually, the crystallographic factor R_F (%) was improved considerably from 20.05% to 8.60% by the above-mentioned methods.

Particle size and dynamical effects. To evaluate dynamical effects related to the accuracy of structure determination, the thickness of $MnFe_2O_4$ nano-crystalline was determined by measuring the average particle size. In order to determine the crystallite sizes of 607 nano-particles shown in Figure 1, the particle finding and analysis were performed by applying the appropriate threshold values with the program analysisSIS (Figure 6a). The $MnFe_2O_4$ crystallites were distributed in the range of 7.8 to 17.8 nm and their average size was about 10.9 nm (Figure 6b). Subsequently, dynamical scattering effects were evaluated by comparing 3 amplitudes: experimental structure-factor amplitudes F_{obs} after the Rietveld refinement, calculated kinematical amplitudes F_{kin}, and calculated

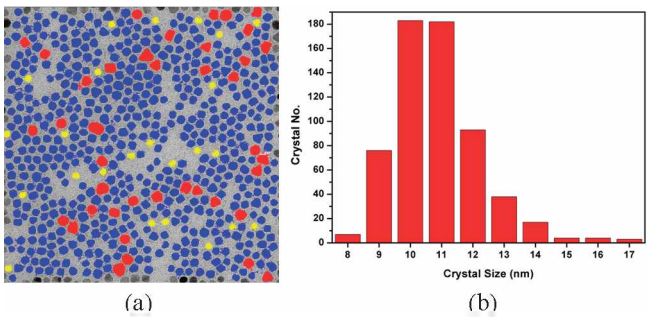

Figure 6. (a) Particle finding and analysis obtained by applying the appropriate threshold values with analySIS program. (b) The size distribution of $MnFe_2O_4$ crystallites is in the range of 7.8 to 17.8 nm and their average size is about 10.9 nm.

dynamical amplitudes F_{dyn}.[13] Dynamical amplitudes F_{dyn} were calculated for the exact Laue condition using the relation[25]

$$F_{dyn} = F_{000}\mathrm{Sin}\left(\frac{\lambda F_{kin} t}{V}\right),$$

where t is the mean thickness of crystallites and the total scattering power per unit cell is F_{000} = 243.6 Å. The electron wavelength λ and cell volume V were taken from Table 1. The ratio of F_{kin} to F_{dyn} is about 1:1.513 and it is expected that the experimental electron diffraction data includes the weak dynamical scattering effects. For a more quantitative and precise study of electron diffraction in a kinematical condition, it is expected that the mean thickness of the crystallites should be about 7 nm at 120 kV.

Alternative methods for relaxation of thickness restriction use high voltage electron microscopy (HVEM) and a newly developed electron diffraction method, precession electron diffraction (PED) method.[26,27] In the study of electron diffraction data by HVEM, dynamical scattering effects are expected to be reduced because of its longer mean free path and extended Ewald sphere by higher transmission power. Application of the PED method is also expected to reduce the dynamical scattering considerably by employing conical beam illumination and rapid precession. For quantitative analysis of single crystal diffraction, PED's effects have been reported in several previous works,[28-30] while PED's effects for the analysis of electron powder diffraction have not been reported yet. Nevertheless, the PED method would be useful to avoid any spotty or discontinuous powder diffraction formed by a small quantity of nano-crystalline which adversely affect for quantitative analysis.

Conclusions

The structure of nano-crystalline $MnFe_2O_4$ was solved and refined by the Rietveld analysis for the electron powder diffraction. The basic crystallographic information of $MnFe_2O_4$ turned out to be space group *Fd-3m*, lattice parameters a = 8.3413(7) Å. These results agree with ICSD-56121 rather than with ICSD-28517 which assumes an initial structure model. The cell parameters and atomic coordinates in the final results coincided with the reference data to within 0.06 Å and 0.01 Å, respectively. Since intensity profiles of electron powder diffraction for nano-crystalline have a steep slope from the center beam and include diffuse scattering intensities from the C-supporting film, it is mandatory to subtract the background intensities reasonably. For a more quantitative structure analysis, effects of preferred orientation should be considered according to the specimen conditions. It is expected that dynamical scattering effects for real nano-structures could be minimized by applying the precession electron diffraction.

Acknowledgments. This work was supported by the Korea Research Council of Fundamental Science & Technology under the STRM project, 2007.

References

1. Caruso, F.; Spasova, M.; Susha, A.; Giersig, M.; Caruso, R. A. *Chem. Mater.* **2001**, *13*, 109.
2. Xiong, Y.; Xie, X.; Chen, S.; Li, Z. *Chem. Eur. J.* **2003**, *9*, 4991.
3. Yu, A.; Mizuno, M.; Sasaki, Y.; Kondo, H. *Appl. Phys. Lett.* **2002**, *81*, 3768.
4. Chaubey, C. S.; Kim, J. *Bull. Korean Chem. Soc.* **2007**, *12*, 2279.
5. Jung, J. S.; Malkinski, L.; Lim, J. H.; Yu, M.; O'Connor, C. J.; Lee, H. O.; Kim, E. M. *Bull. Korean Chem. Soc.* **2008**, *29*, 758.
6. Gillot, B. *Eur. Phys. J. Appl.* **1998**, *4*, 243.
7. Sugimoto, M. *J. Am. Ceram. Soc.* **1999**, *82*, 269.
8. Tang, Z. X.; Sorensen, C. M.; Klabunde, K. J.; Hadjipanayis, G. C. *Phys. Rev. Lett.* **1991**, *67*, 3602.
9. Kulkarni, G. U.; Kannan, K. R.; Arunarkavalli, T.; Rao, C. N. R. *Phys. Rev. B* **1994**, *49*, 724.
10. Van der Zaag, P. J.; Brabers, V. A.; Johnson, M. T.; Noord-ermeer, A.; Bongers, P. E. *Phys. Rev. B* **1995**, *51*, 12009.
11. Lee, J. H.; Huh, Y. M.; Jun, Y. W.; Seo, J. W.; Jang, J. T.; Song, H. T.; Kim, S.; Cho, E. J.; Yoon, H. G.; Suh, J. S.; Cheon, J. *Nature Medicine* **2007**, *13*, 95.
12. Weirich, T. E.; Winterer, M.; Seifried, S.; Hahn, H.; Fuess, H. *Ultramicroscopy* **2000**, *81*, 263.
13. Weirich, T. E.; Winterer, M.; Seifried, S.; Mayer, J. *Acta Cryst.* **2002**, *A58*, 308.
14. Cheon, J.; Seo, J. W.; Lee, J. H. *Korea Patent PCT* **WO2006/** 052042.
15. Roisnel, T.; Rodriguez-Carvajal, J. *WINPLOTR, a New Tool for Powder Diffraction*; Laboratoire Leon Brillouin: CEA-Saclay, France, 2000.
16. CRYFIRE is written by Shriley, R. et al., and distributed free for non-profit use from the CCP14 website: *http://www.ccp14.ac.uk/tutorial/crys*
17. CHECKCELL is written by Laugier, J. & Bochu, B. and distributed free from the CCP14 website: *http://www.ccp14.ac.uk/tutorial/lmgp/*
18. Koenig, U.; Chol, G. *J. Appl. Cryst.* **1968**, *1*, 124.
19. Rodriguez-Carvajal, J. *FULLPROF-A program for Rietveld, profile matching and integrated intensities refinement of X-ray and/or neutron data*; Laboratoire Leon Brillouin: CEA-Saclay, France, 2000.
20. Jiang, J. S.; Li, F. H. *Acta Phys. Sin.* **1984**, *33*, 845.
21. Thomson, P.; Cox, D. E.; Hasting, J. B. *J. Appl. Cryst.* **1987**, *20*, 79.
22. Holgersson, S. *Lunds Univ. ÅrssKrift, N. F., Avd. 2* **1927**, *23*, 9; *Kungl. Fysiogr. Sällsk. Handl., N. F.*, 38, 9.
23. Wang, J.; Chen, Q.; Hou, B.; Peng, Z. *Eur. J. Inorg. Chem.* **2004**, 1165.
24. Deng, H.; Li, X.; Peng, Q.; Wang, X.; Chen, J.; Li, Y. *Angew. Chem.* **2005**, *117*, 2.
25. Cowely, J. M. *International Tables for Crystallography*; Kluwer Academic Publishers: Dordrecht, 1999; Vol. C, pp 80-82, 259-262.
26. Vincent, R.; Mldgley, P. A. *Ultramicroscopy* **1994**, *53*, 271.
27. Weirich, T. E.; Portillo, J.; Cox, G.; Hibst, H.; Nicolopoulos, S. *Ultramicroscopy* **2006**, *106*, 164.
28. Boulahya, K.; Ruiz-Gonzalez, L.; Parras, M.; Gonzalez-Calbet, J. M.; Nickolsky, M. S.; Nicolopoulos, S. *Ultramicroscopy* **2007**, *107*, 445.
29. Dorset, D. L.; Gilmore, C. J.; Jorda, J. L.; Nicolopoulos, S. *Ultramicroscopy* **2007**, *107*, 462.
30. Oleynikov, P.; Hovmoller, S.; Zou, X. D. *Ultramicroscopy* **2007**, *107*, 523.